Journal of Physics:
Conference Series

PAPER • OPEN ACCESS

Nacelle-based lidar measurements of wind farm turbulence and validation with a fleet of multicopter drones

To cite this article: Norman Wildmann *et al* 2026 *J. Phys.: Conf. Ser.* **3224** 022031

Journal of Physics: Conference Series **3224** (2026) 022031 doi:10.1088/1742-6596/3224/2/022031

Nacelle-based lidar measurements of wind farm turbulence and validation with a fleet of multicopter drones

Norman Wildmann[1], **Julia Menken**[1] **and Johannes Kistner**[1,2]

[1] Deutsches Zentrum für Luft- und Raumfahrt e.V., Institut für Physik der Atmosphäre, Oberpfaffenhofen, Germany

[2] Carl von Ossietzky Universität Oldenburg, School of Mathematics and Science, Institute of Physics

E-mail: `norman.wildmann@dlr.de`

Abstract. Measuring atmospheric turbulence in spatially heterogeneous environments, such as wind farms, presents a significant observational challenge. This study aims to enable and validate turbulence measurements derived from a nacelle-based Doppler Wind Lidar (DWL). We present a refined measurement methodology and validate it against simultaneous in situ reference data collected by a fleet of ten drones and sonic anemometers mounted on meteorological masts at the WiValdi research park.

A comparative analysis of a multi-hour case study under moderately non-stationary conditions — including the onset of wind turbine wakes — yields deviations between the remote sensing and in situ systems that are on the order of the drone fleet's measurement uncertainty. This demonstrates the high potential of the lidar-based approach. We observe that in wake flow conditions, distinctions between geodetically fixed and turbine-fixed reference frames can lead to divergences in measurement comparisons. Despite these challenges, the lidar estimates prove robust. The resulting spatial maps successfully resolve variations in turbulence intensity across different regions, specifically enabling accurate turbulence estimation within waked wind farm flows.

1. Introduction

Atmospheric turbulence is a grand challenge in achieving optimal wind turbine performance and reliability, as highlighted by Veers et al. [1]. The flow's non-Gaussian, non-stationary, and inhomogeneous nature — particularly at scales of a few to a few hundred meters — significantly impacts the design loads and control of both individual turbines and entire wind farms. Furthermore, ambient turbulence is well-known to have a major influence on wind turbine wakes and their decay, a topic extensively studied through large-eddy simulations (LES) [2–4]. While LES provides valuable insights, such numerical studies require rigorous validation with full-scale experimental data. Lidar remote sensing has become the primary technique for continuously observing wind profiles and atmospheric turbulence through the atmospheric boundary layer (ABL) [5–7]. Specifically, scanning Doppler wind lidars (DWL) have been used extensively to characterize wind turbine wakes [8–10]. Most often, horizontal plan position indicator (PPI) scans are conducted for this purpose and in best case from top of a wind turbine nacelle or some other elevated platform which allow far scans of the flow at constant (hub) height. The big advantage of such scans is, that they provide spatial and temporal information about the wind field. A key challenge remains: accurately estimating representative turbulence from DWL measurements, given the inherent limitations of the measurement principle, such as spatial and temporal averaging and the limited temporal resolution of successive scans. While a multitude of methods exist for profiling lidars to determine vertical profiles of turbulence [7, 11], only few make use of the Doppler spectral broadening to adequately correct for the spatial averaging effect [12]. We here refine the method based on Wildmann et al. (2019) [13] to generate two-dimensional maps of velocity variance within the PPI scanning area of a nacelle-mounted DWL. The results are validated with in situ measurements from sonic anemometers on meteorological masts and a fleet of small multicopter uncrewed aerial systems (UAS), also known as drones, the SWUF-3D fleet, which has been proven to measure accurate 3D turbulence in the past [14] and can be operated safely in the vicinity of operating wind turbines [15]. Our work demonstrates the potential of this DWL-based method to not only obtain background turbulence, but also spatially resolved maps of turbulence in highly non-homogeneous flows such as wind turbine wakes. At the same time we want to raise awareness of the challenges for spatial variance estimates in the highly transitional flows found in wind farms and the uncertainties associated with the choice of the scanning strategy. In Sect. 2 we describe how velocity variance is determined from DWL PPI scans and how the parameters for comparison are estimated from in situ observations by drone and sonic anemometer. Sect. 3 presents all results from our case study and Sect. 4 provides a summary and outlook for the work.

2. Methods

This study combines measurements from scanning DWL, sonic anemometers on meteorological masts and drone-based measurements. In this section, we briefly introduce the experimental setup and the data processing to allow comparative measurements.

2.1. Experiment description

Measurements for this study were carried out at the Krummendeich research park WiValdi in northern Germany (`https://windenergy-researchfarm.com/`). The site features two 4.2 MW wind turbines of type Enercon E-115 (OPUS1 and OPUS2) which are aligned in main wind direction, which is typically from west-southwest [16]. On the generator platform of OPUS1, a Leosphere Windcube 200S DWL has been installed since 2023 to measure the flow downstream of the turbine. In March 2025, the SWUF-3D drone fleet was deployed at the site primarily to carry out spatially simultaneous measurements in the wake of OPUS1. In those times when OPUS1 was not operating, basic wind field and turbulence measurements were carried out. We focus on a specific case study: on 25 March 2025, OPUS1 was not operating but facing west for multiple hours, so that measurements from the nacelle lidar were made in between OPUS1 and OPUS2 without a significant wake and the SWUF-3D drone fleet was measuring in this same area. Four flights were done with a flight pattern aligning ten drones in 20 m separation between the turbines at hub height (z_h=92 m). We refer to this scenario as 10x1 pattern. Three more flights were done with five drones at 92 m and five drones at 50 m with 40 m horizontal separation, aligned with main wind direction towards the MMA between 15:00 and 17:00. We refer to this scenario as 5x2 pattern, but only use the five drones at hub-height in this study. Just after 16:30 UTC, OPUS1 started operating and the SWUF-3D fleet was set up to take measurements within the wake with a setup similar to the one shown in Wildmann and Kistner (2025) [17]. Five drones are positioned at a downstream distance of one rotor diameter ($y_w = D$, with index w for the wind turbine coordinate system), measuring the flow field at hub height in five lateral positions ([-D/2, -D/4, 0, D/4, D/2]). At y_w=0.5D and y_w=1.5D downstream, two more drones each are placed at x_w=[-D/2, D/2]. We refer to this scenario as the wake

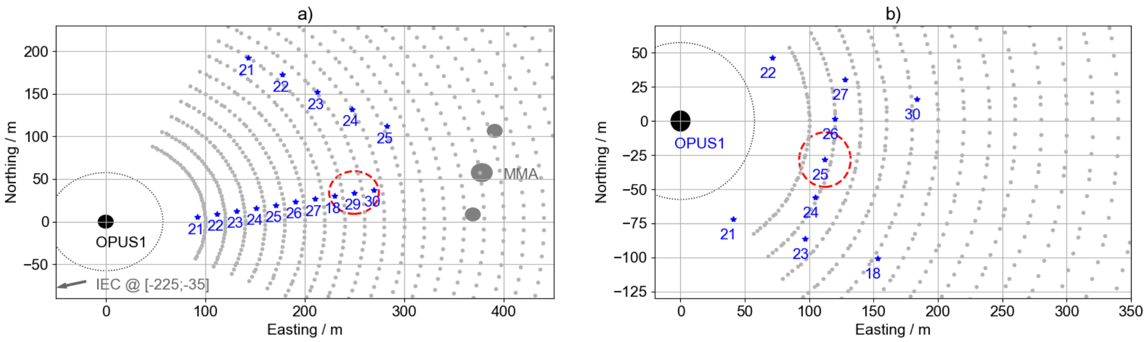

Figure 1. Map of the measurement layout for 25 March 2025. The black dot shows the wind turbine OPUS1 surrounded by a dashed circle with a diameter equal to the rotor diameter. Light grey dots indicate the range gate center points for the lidar measurements from the nacelle-based lidar and the blue stars indicate the positions of the SWUF-3D drones with the individual drone numbers below. Panel a) shows the 10x1 and 5x2 pattern and panel b) the wake pattern. The red dashed circle gives an example of the area that is used for a variance retrieval from the lidar scan.

pattern. Figure 1 shows all of the pattern as blue stars with respective drone numbers on a map in the geodetic coordinate system centered to the OPUS1 wind turbine location. The individual measurements of the lidar are indicated as light grey dots and the meteorological mast array (MMA) as dark grey circles. Not on the map is the inflow mast, which we refer to as IEC mast, as it is instrumented to allow meteorological measurements according to the IEC standards. The IEC mast is located at a distance of 600 m and an angle of 260° from the center mast of the MMA.

Figure 2 shows the wind speed U (a), the wind direction Ψ (b), the velocity variance σ_v^2 (d), the stationarity index s_i (e) and integral length scale of turbulence L for the observational period (see Sect. 2.4 and 2.6 for details on the latter two). Figure 2c qualitatively shows the power production by OPUS1 and the time periods of UAS observations with the respective pattern. The whole day can be separated into three main phases: First, from 12:00—14:00 UTC, a period of westerly winds with high turbulence, second, a phase with lower turbulence and north-westerly winds from 14:30–16:30 UTC and last, a phase with operating wind turbine OPUS1 and increased turbulence after 16:30 UTC. In phase 1, the wind direction is in line with the two masts and they both show almost equal horizontal velocity U. As soon as the wind turns in phase 2, some difference between the wind speeds at the two sonics can be observed up to a magnitude of 0.5 m s^{-1}. This is possibly due to inhomogeneity in the inflow with some rows of trees in westerly direction. In phases 1 and 2, the flow is moderately non-stationary, and L is somewhat elevated, likely due to transitional periods in the averaging periods. In phase 3, the MMA is affected by the wind turbine wake, which shows in variance, stationarity and integral length scale.

2.2. Nacelle-based lidar measurements

The Windcube 200S lidar installed on OPUS1 was configured to scan the flow field downstream of OPUS1 in horizontal planes at 5 different elevation angles, i.e. $\varphi = [-14°, -7°, 0°, 7°, 14°]$ [18]. In this study we focus on the 0°-elevation scan and remove all other scans from the dataset.

As described in Wildmann et al. (2020) [19], spatial scans with DWL can be used to calculate the total variance of the flow σ_v^2 in defined spatial boxes using the variance of line-of-sight (LOS)

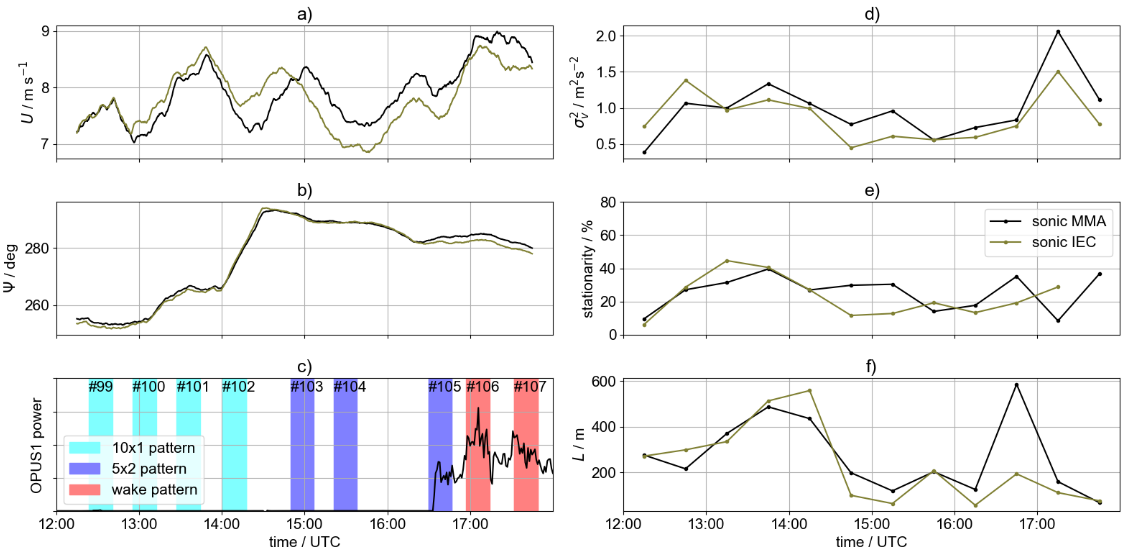

Figure 2. Experimental conditions on 25 March 2025. Shown are wind speed U (a) and wind direction Ψ (b) as measured by sonic anemometers on the IEC mast and the MMA. Panel (c) shows the turbine power variation and the time slots for drone measurements with the corresponding flight numbers (#99-#107). Panels (d-f) show derived 30-minute averages of variance σ_v^2, stationarity index s_i and integral length scale L respectively.

velocities $\hat{\sigma}_v^2$ and the turbulent broadening of the Doppler return spectrum σ_t^2. The top hat in $\hat{\sigma}_v^2$ indicate that these are direct measurements from the lidar, whereas σ_t is a derived variable. The threshold between resolved turbulence in the line-of-sight velocities and the contribution of σ_t^2 is defined by the pulse-averaging. The transfer function H_p of the low-pass spatial filter of the lidar, is simplified here to a Gaussian function, so that

$$H_p(\kappa) = \exp\left(-2\pi(\Delta z \kappa)^2\right) \quad , \tag{1}$$

with κ the wavenumber and Δz the length of the averaging window. Mulitplied with the variance spectrum S_v, the variance contributions can then be calculated as the integral under the filtered spectra as:

$$\hat{\sigma}_v^2 = 2\int_0^\infty d\kappa S_v(\kappa) H_p(\kappa) \quad , \tag{2}$$

$$\sigma_t^2 = 2\int_0^\infty d\kappa S_v(\kappa)\left[1 - H_p(\kappa)\right] \quad . \tag{3}$$

The total variance of the LOS velocity σ_v^2 is the sum of measured variance $\hat{\sigma}_v^2$, turbulent broadening of the spectra σ_t^2 and an error term accounting for instrumental noise σ_e^2:

$$\sigma_v^2 = \hat{\sigma}_v^2 + \sigma_t^2 + \sigma_e^2 \quad . \tag{4}$$

For the turbulent broadening term, it is important to recognize that shear within the averaging volume $\hat{\sigma}_s^2$ can have a significant contribution, especially in wake measurements with strong velocity gradients and needs to be subtracted from the measured spectral width $\hat{\sigma}_{\mathrm{sw}}^2$, along with the baseline spectral width at zero velocity σ_0:

$$\sigma_t^2 = \hat{\sigma}_{\mathrm{sw}}^2 - \sigma_0^2 - \hat{\sigma}_s^2 \tag{5}$$

Table 1. DWL characteristics and settings

parameter	variable name	value
installation height	z_{hub}	95 m
physical volume	Δz	35 m
zero-velocity spectral width	σ_0^2	0.5 $\mathrm{m^2 s^{-2}}$
azimuth	θ	-45...45°
elevation	φ	$[-14°, -7°, 0°, 7°, 14°]$
angular resolution	$\Delta\theta$	2°
single-elevation scan duration	Δt_s	7 s
scan repetition rate	Δt_0	52 s

For best accuracy of the line-of sight variance $\hat{\sigma}_v^2$, all relevant scales of turbulence should be included in the estimate, either through temporal or spatial averaging. In this study, the repetition rate of LOS measurements at the same point is limited to approximately once every 52 s due to the multiple elevation angles that were scanned. Also, since we want to be able to show spatial differences in turbulence at different positions in a wind farm, we want to keep the area for spatial averaging relatively small and set it to a radius of dr=25 m around the points of interest. This area is indicated in Fig. 1 as a red dashed circle around a drone position. It is not possible to obtain measurements exactly at the mast position, as the mast structure, booms and guy wires cause a lot of hard target reflections that significantly disturb the lidar measurements. Therefore, the indicated position upstream at the position of UAS#29 in the 10x1 pattern is used for single-point comparisons between lidar and mast. Table 1 provides details about the lidar configuration.

2.3. SWUF-3D drone fleet

The SWUF-3D multicopter drone fleet has been deployed in multiple campaigns in boundary-layer meteorology [20] and wind energy research [17]. Its unique feature to sample highly resolved 3D information of the flow simultaneously at up to 20 points in space makes it a powerful tool to sample turbulent features in the ABL. For the in situ measurements by the drones, we can directly calculate σ_v^2 as the variance of the horizontal wind velocity for hover periods. In this campaign, the hover period duration was between 12 and 15 minutes. The wind vector is estimated from avionics data without any additional sensor and achieves an accuracy well below 0.5 m $\mathrm{s^{-1}}$. Wind direction was estimated to be within an accuracy of ±5° in previous campaigns, but is dependent on the location of the measurements and magnetic field calibration. For temperature and humidity, a self-built sensor is installed on each drone. With a temporal resolution of 2 Hz, the drones provide a good reference to evaluate the lidar-based turbulence estimates. In this study, we set the sampling frequency to 5 Hz. The fleet performs all flights automatically with pre-defined flight tracks. The flight pattern can be adjusted between each flight according to the wind direction.

2.4. Meteorological mast measurements

Two sonic anemometers are used for the analyses. A METEK uSonic-3 Cage MP at the IEC at 85 m height and a THIES 3D (4.3830.20.340) at the central mast of the MMA at 100 m height above ground. Data of both sonic anemometers are corrected for misalignment with respect to the meteorological coordinate system. We use these measurements to determine the background situation at the research park. In half-hour intervals, we determine the stationarity index according to Foken and Wichura (1996) [21] and the integral length scale L from the autocorrelation function [22]. Further, we mimic the lidar-measured variance component σ_t^2

Journal of Physics: Conference Series **3224** (2026) 022031 doi:10.1088/1742-6596/3224/2/022031

through a filter in the frequency domain that is applied to the sonic measurement's variance spectrum S according to Eq. 3.

2.5. Coordinate frames and synchronization

The experimental campaign utilizes a coordinated setup involving a wind turbine-mounted lidar and drones to characterize inflow turbulence. The lidar is positioned in the wind turbine fixed coordinate system, rotating dynamically with the turbine's yaw angle, Ψ_w. Figure 3 shows a sketch of the coordinate systems and a picture of the setup in the field.

A critical challenge is the alignment of the two independent measurement systems. The lidar performs PPI (Plan Position Indicator) scans to measure radial wind velocity. For the lidar turbulence analysis, we need to assume isotropic turbulence, since lidar beam directions vary over a scan. For best validation, we nevertheless attempt to use the same wind component from lidar, drone and sonic. Therefore, the three-dimensional wind measurement from the drone and sonic are projected onto the lidar beam direction and for each scan, the lidar beam closest to the reference instrument can be selected. For the projection of the in situ wind vector onto the lidar line-of-sight, the elevation angle φ of the lidar beam is neglected. This simplification assumes a horizontal scanning plane, meaning only the horizontal wind components of the drone data are projected onto the lidar's azimuthal direction. The projection angle is a superposition of the wind turbine yaw angle Ψ_w and the lidar azimuth angle θ. The wind turbine coordinate system is pointing towards the wind. Since we want the wind component in LOS direction of the backward-facing lidar, we have to subtract 180°. Also, the lidar coordinate system is oriented to negative Y_w, so that the projection angle yields $\theta_p = \Psi_w - 180° - 90° + \theta$ and the projection vector:

$$\mathbf{n}_{LOS} \approx \begin{pmatrix} \sin\theta_p \\ \cos\theta_p \\ 0 \end{pmatrix} \tag{6}$$

$$\tag{7}$$

The final projected velocity can then be easily obtained as:

$$\begin{aligned} v_p &= \mathbf{u}\cdot\mathbf{n}_{LOS} \\ v_p &= u\sin(\theta_p) + v\cos(\theta_p) \end{aligned} \tag{8}$$

2.6. Turbulence parameters

We focus in this study on flow velocity variance σ_v^2 as the primary variable for turbulence:

$$\sigma_v^2 = \frac{1}{N-1}\sum_{i=1}^{N}(v_i - \overline{v})^2 \tag{9}$$

All data is removed from linear trends prior to calculating the variance.

A stationarity index s_i is calculated based on the variance estimates of the full 30-minute period in relation to 5-minute sub-periods and expressed in percentage:

$$s_i = \left| \frac{\frac{1}{6}\sum_{i=1}^{6}(\sigma_{v,5}^2)_i - \sigma_{v,30}^2}{\sigma_{v,30}^2} \right| * 100\% \tag{10}$$

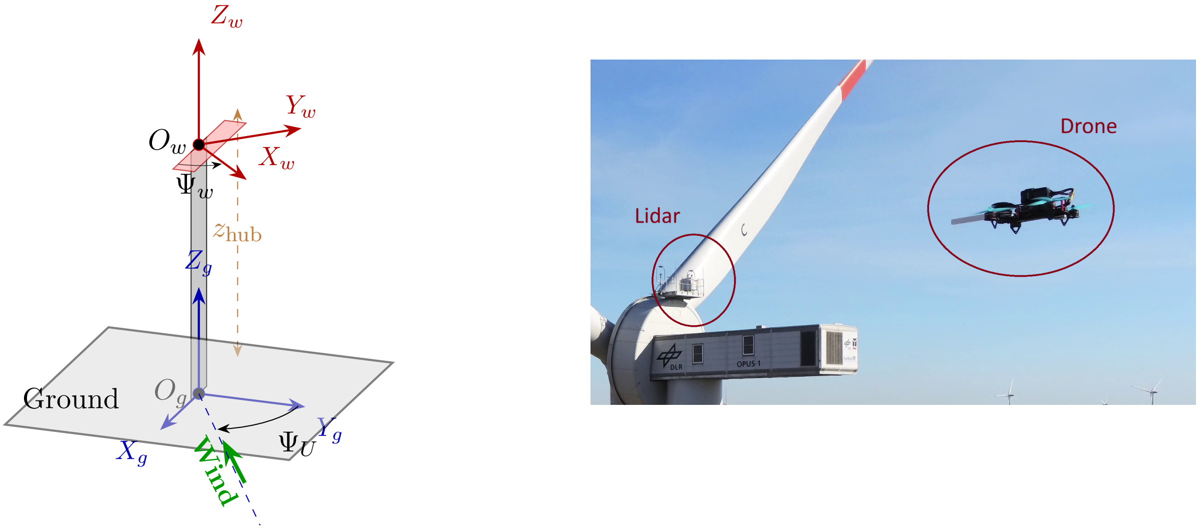

Figure 3. Reference frames for wind turbine. The figure shows the transformation from the geo-fixed ground system $\{g\} = (X_g, Y_g, Z_g)$=(East, North, Up) to the wind turbine frame $\{w\} = (X_w, Y_w, Z_w)$. The transformation involves a translation by the hub height z_{hub} and a rotation by the yaw angle Ψ_w about the vertical Z-axis. The wind direction is indicated as the clock-wise angle from north (Y_g).

3. Results

3.1. Validation of lidar variance

Figure 4a shows the results of the comparison of lidar-derived turbulence and drone-based measurements for 25 March 2025 over a period of multiple hours and the full measurement domain. The light red lines are estimates for a 25 m grid in the area between OPUS1 and MMA as shown in Fig. 1. The three phases of the observational period can be nicely seen. Before 16:30, OPUS1 was not operating. The transition phase to a waked flow shows cleary in the variation of variance in the spatial measurements. During the time without turbine operation, the lidar estimates match the drone observations fairly well. The largest deviations are in periods with high instationarity and transitional phases, e.g. at 13:30 UTC. The higher measurements of the drones at 15:00 UTC can be attributed to the different measurement location for the 5x2 pattern and the shifted wind direction in that period. The last two drone fleet flights are done with the wake pattern. It is obvious that the variation of the variance observation depending on the location of the drone differs considerably in that case. This is also reflected in the variation between lidar estimates at different positions.

Figure 4b gives the lidar estimate in red stars only at the location of UAS#29 in the 10x1 pattern and additionally shows the measurements from the sonic anemometers at the two masts. In comparison to Fig. 2, we now reduced the averaging time to 15 minutes to match the drones and applied a moving window with 5-minute steps for better temporal resolution. The difference between MMA and IEC at 15:00 UTC indicate a large spatial inhomogeneity during that period. In the first period with the four 10x1 pattern UAS flights, measurements match well, except for flight #100, and are within the margin of error of 0.16 $\mathrm{m^2s^{-2}}$ that were previously determined for the drones [14]. The root-mean-squared error (RMSE) between the average of the drone fleet and the temporally matching lidar estimates of the MMA yields 0.15 $\mathrm{m^2s^{-2}}$. In order to understand the contribution of scales to the total variance, we also show the turbulent broadening σ_t^2 as determined for the lidar (red crosses) and the corresponding sonic equivalent (dashed lines). For the majority of the time, these values are very small, on the order of 0.1 $\mathrm{m^2s^{-2}}$. Only during

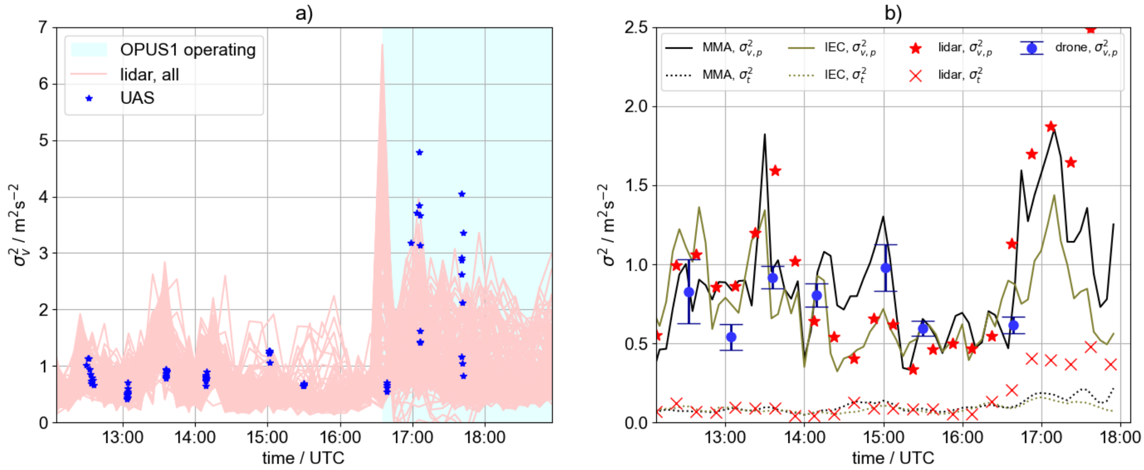

Figure 4. a) Variance σ_v^2 as estimated from lidar along lines of sight (light red lines) over the full area and drones for horizontal wind speed (blue stars). The times when OPUS1 was operating are shaded in light blue. b) Projected variance $\sigma_{v,p}^2$ as estimated from lidar at the reference point (red stars) and drone fleet (blue dots with standard deviation of the fleet as error bars). The black and orange line give sonic anemometer estimates from the MMA and IEC respectively. Dashed lines and red crosses give the small-scale turbulence part as measured by lidar (red crosses) and sonic (dashed lines).

the wake period, values are significantly elevated, and even more so for the lidar than the sonic. This makes sense, as the wake hits the position of the lidar estimate more directly, the IEC mast not at all and the MMA at a position further downstream. Not shown in Fig. 4b are the two wake pattern flights from the drones, since the variances of each single drone at its specific location within the wake vary significantly and an average is not very meaningful. Details about the distribution of variance within the wake are given in the next section.

3.2. Wake flow

For the two wake pattern flights with the SWUF-3D fleets on 25 March 2025, we match the location of variance estimation from the lidar exactly with the five central drones at 1 D downstream (see Fig. 1b, UAS#23-27). The results for variance at these locations are shown in Fig. 5a in comparison of the UAS and the lidar for the two selected flights. For the last flight (#107), a very good agreement is found with deviations below the measurement uncertainty. During the prior flight (#106), some more yaw motion of the wind turbine was happening and thus the drone estimates show a larger variance, since the high resolution measurements are more effected by the exact position within the wake. The dashed lines in the plot show the variance as measured at the masts. The MMA seems to be effected by the wake somewhat during flight #107, whereas during flight #106, both masts are showing almost identical values. The results give confidence that the lidar estimates are robust enough for quantitative wake turbulence determination. In Fig. 5b, we show the full map of turbulence estimates from the lidar PPI with an oversampled resolution of 10 m in both, x- and y-direction. It nicely shows how the highest variance is found in the near wake and quickly fades into a significantly reduced turbulence level in the far wake, which is however still elevated compared to the background. In the upper right corner of the image, wake turbulence of the neighboring turbine OPUS2 can be seen.

Journal of Physics: Conference Series **3224** (2026) 022031 doi:10.1088/1742-6596/3224/2/022031

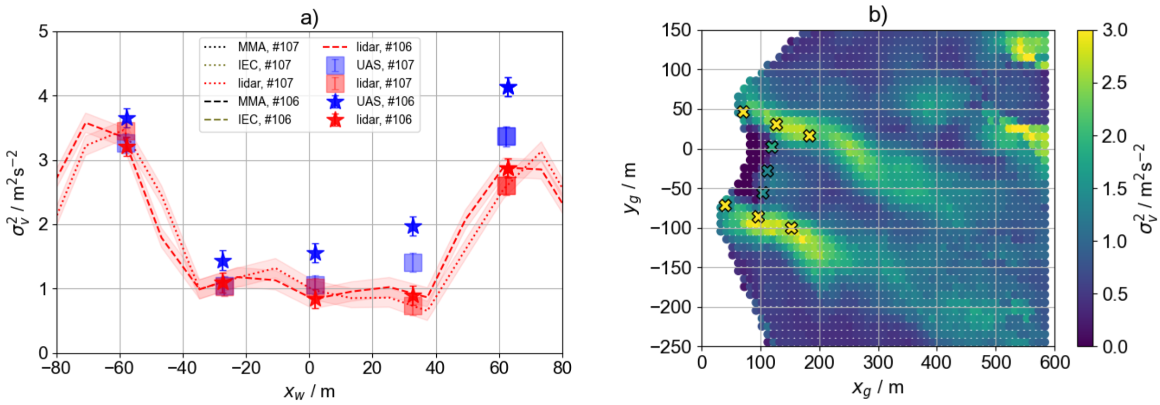

Figure 5. a) Variance at different x-positions in the turbine-fixed coordinate system for flights #106 (stars, dashed lines) and #107 (squares, dotted lines), as measured from drones (blue) and lidar (red). The background level is shown with measurements of the sonic in the inflow (IEC, orange) and at the MMA (black). b) The full map of the lidar PPI variance estimate in the geodetic coordinate system centered in OPUS1 for flight #106. The crosses give the measurements by the drones at the hover locations in the wake.

4. Conclusion and Outlook

This work presented a comprehensive case study analyzing one day of simultaneous turbulence measurements using a nacelle-based Doppler Wind Lidar (DWL) and a fleet of drones at the WiValdi research park. The primary objective was to assess the capability of remote sensing techniques to capture complex flow dynamics in a wind farm environment.

Our study demonstrates that variance estimates obtained from nacelle-based DWL — specifically those derived from LOS variance and spectral broadening — have the potential to provide accurate values of second-order statistics. This holds true for both undisturbed inflow and the complex, waked situations typical of wind farms. A quantitative comparison revealed that the deviations between the remote sensing estimates and the in situ sonic anemometer and drone measurements are on the order of the measurement uncertainty, approximately $0.15\,\mathrm{m^2s^{-2}}$. Larger differences can in most cases be explained with spatial separation of the measurement locations.

The deployment of a drone fleet proved highly valuable for validating lidar estimates across different points within the scanning area. This validation is particularly critical in the highly inhomogeneous environment of a wind farm, where flow properties change rapidly over short distances. However, the study also highlighted significant challenges regarding the synchronization of time and space between moving platforms. In strongly transitional flows, such as the wake region, even minor discrepancies in spatiotemporal alignment can lead to errors in the comparison of measurement techniques. Consequently, while nacelle-based scanning lidar is a powerful tool for estimating turbulence, validation requires rigorous processing of both lidar and in situ data, with particular attention paid to non-stationary conditions.

While these initial results are promising, the analysis of a single day constitutes only a first step. A significantly larger volume of available data will be analyzed in future to provide a robust qualification of the method's accuracy. This future work can systematically investigate potential sources of error, specifically focusing on the anisotropy of turbulence and the difficulty of disentangling mean shear from actual turbulence in lidar scans.

Operational lessons learned suggest that for effective turbulence measurements, the repetition frequency of lidar scans should be high, if at the same time the spatial averaging domain should be small. This is particular critical for wake studies, with turbulent features manifesting on small scales. Furthermore, because strong velocity gradients in the wake manifest as spectral broadening of the Doppler return signal, it is essential to correct measurements for these shear contributions to achieve a clear separation of scales.

Finally, the physical interpretation of wake turbulence requires careful consideration of the reference frame. We observed potentially large differences between estimates calculated in the wind turbine coordinate frame versus the geodetic coordinate frame. While the geodetic frame is likely more relevant for load estimation, the wind turbine frame may offer better insights into the basic understanding of wake dynamics. Moreover, simple metrics like velocity variance and turbulence intensity may not be adequate to describe the flow — and ultimately the loads on turbines — without considering the spectral distribution of energy. To address the role of spatial organization in these flows, future analyses could employ advanced processing methods, such as the wavelet-based techniques presented in [23].

Acknowledgments

This research has been supported by the HORIZON EUROPE European Research Council (grant no. 101040823, ESTABLIS-UAS). This work was supported by the Federal Ministry for Economic Affairs and Energy on the basis of a decision by the German Bundestag (NearWake FKZ 01258365/1). We acknowledge the support by the DLR-WX team during the campaign, in particular Jakob Klassen, Jan-Simon Hesse and Julian Klein. We also thank Almut Alexa, Lukas Bührend and Jeffrey Thayer for their hard work in preparing and carrying out the campaign at Krummendeich. The authors acknowledge the use of a large language model (e.g., Gemini) for language improvements.

References

[1] Veers P 2023 *Wind Energy Science* **8** 1071–1131
[2] Wu Y T and Porté-Agel F 2012 *Energies* **5** 5340–5362 ISSN 1996-1073
[3] Englberger A and Dörnbrack A 2018 *Boundary-Layer Meteorology* **166** 423–448
[4] Parinam A, Benard P, Von Terzi D and Viré A 2024 *Journal of Physics: Conference Series* **2767** 092098
[5] Smalikho I, Köpp F and Rahm S 2005 *Journal of Atmospheric and Oceanic Technology* **22** 1733–1747
[6] Frehlich R and Kelley N 2008 *IEEE Journal of Selected Topics in Applied Earth Observations and Remote Sensing* **1** 42–47 ISSN 1939-1404
[7] Wildmann N, Päschke E, Roiger A and Mallaun C 2020 *Atmospheric Measurement Techniques* **13** 4141–4158
[8] Iungo G V, Wu Y T and Porté-Agel F 2013 **30** 274–287
[9] Iungo G V and Porté-Agel F 2014 *Journal of Atmospheric and Oceanic Technology* **31** 2035–2048
[10] Wildmann N, Kigle S and Gerz T 2018 *Journal of Physics: Conference Series* **1037** 052006
[11] Sathe A and Mann J 2013 *Atmospheric Measurement Techniques* **6** 3147–3167
[12] Manami M, Mann J, Sjöholm M, Léa G and Gorju G 2025 *Atmospheric Measurement Techniques* **18** 7513–7523
[13] Wildmann N, Bodini N, Lundquist J K, Bariteau L and Wagner J 2019 *Atmospheric Measurement Techniques* **12** 6401–6423
[14] Wetz T and Wildmann N 2022 *Journal of Physics: Conference Series* **2265** 022086

[15] Wildmann N and Győry L 2025 *Atmospheric Measurement Techniques* **18** 5527–5544

[16] Wildmann N, Hagen M and Gerz T 2022 *Journal of Physics: Conference Series* **2265** 022029

[17] Wildmann N and Kistner J 2025 *Journal of Physics: Conference Series* **3016** 012011

[18] Menken J and Wildmann N 2026 *Wind Energy Science Discussions* **submitted**

[19] Wildmann N, Gerz T and Lundquist J K 2020 *Journal of Physics: Conference Series* **1618** 032034

[20] Wetz T, Zink J, Bange J and Wildmann N 2023 *Boundary-Layer Meteorol* **187** 673–701 ISSN 1573-1472

[21] Foken T and Wichura B 1996 *Agricultural and Forest Meteorology* **78** 83–105

[22] Pope S B 2011 *Turbulent flows* (Cambridge: Cambridge Univ. Press)

[23] Lengyel J 2025 The spatial organization of wind turbine wakes (*Preprint* `2512.14804`)